SPE-203421-MS

Hydrocarbon Findings in Challenging Shilaif in Western UAE Core Analysis Approach

David Gonzalez, Osama Al Jallad, and Kresimir Vican, Halliburton; Abdula Al Blooshi, Maryam Al Shehhi, Ashis Shashanka, and Anoop Mishra, Al Yasat Petroleum

This paper was prepared for presentation at the Abu Dhabi International Petroleum Exhibition & Conference to be held in Abu Dhabi, UAE, 9 – 12 November 2020. Due to COVID-19 the physical event was changed to a virtual event. The official proceedings were published online on 9 November 2020.

Abstract

Cenomanian carbonate deposits of Shilaif Formation, located west of Abu Dhabi, exhibit a high degree of heterogeneity at multi scales. To characterize this formation and explore its hydrocarbon potential, several geological, petrophysical, and geochemical analyses, including digital rock analysis (DRA), were applied and integrated.

A hundred ft of whole core were logged at the surface using dual-energy X-ray CT (DECT) and Spectral Gamma (SGR) to generate bulk density, photoelectric factor, and gamma logs. Based on integration between DECT, SGR, and wireline logs, high-resolution total organic carbon (TOC), brittleness index, and mineralogy logs were generated at a millimeter scale, and representative core samples were extracted. Inorganic and organic geochemical analyses represented by X-ray diffraction, LECO TOC, HAWK pyrolysis, vitrinite reflectance, and hydrocarbons chromatography (SARA) were performed on selected samples to define rock mineralogy, type, and degree of organic matter maturity and chemical composition of the hydrocarbons. Nuclear magnetic resonance (NMR) at native, dry and full-brine saturation conditions, mercury injection capillary pressure (MICP), and crushed rock analysis (CRA) were conducted on selected samples to determine fluid saturations, porosity, permeability, and pore-throat-size distribution. The pore-scale analysis was also performed using argon-ion-milled SEM images to quantify organic matter contents and total, effective, and organic matter porosities. All core data obtained at multiscale were integrated with the wireline and generated high-resolution logs to validate and select optimal horizontal leg landing zones.

DECT and SGR logs showed the top of Shilaif is mainly made of calcite, while its bottom is calcitic with minor concentrations of clay minerals and pyrite. Integration between DECT and SGR logs showed the mid and bottom of the formation have high radioactivity attributed to the presence of organic matter in intermediate concentrations and the presence of clay minerals. Pyrolysis analysis indicated a kerogen type I to II with an average Tmax equal to 431°C. Measured and calculated vitrinite reflectance (Ro) was, on average, 0.59, confirming that the kerogen of Shilaif in the area of study falls within the immature to the early mature oil window. Measurements such as CRA, MICP, NMR, and 2D SEM analyses showed that Shilaif has low porosity of approximately 3% on average and very low permeability averaging 0.00057 mD. The 2D SEM images and NMR data confirmed this and revealed that it lacks the porosity associated with

the organic matter resulting from its low degree of transformation. Lab data and upscaled petrophysical logs showed that Shiliaf in this field has a low degree of thermal maturity and fall within the early oil window.

Integration between core analysis results and wireline data helped understand the Shilaif Formation characteristics and determine its hydrocarbon potential. It also provided additional calibration to the wireline data.

Introduction

In the last few years, the unconventional oil and gas source rocks have become a vital and attractive source of hydrocarbons production globally, especially in the USA and Saudi Arabia. In the UAE, recently, several new onshore wells have been drilled in the Western of Abu Dhabi to explore the potential unconventional source rocks, particularly within the Cenomanian carbonate deposits of Shilaif Formation (Steiner et al. 2015).

Shilaif Formation comprises the upper part of the Wasia Group, as shown in the UAE's stratigraphic column in Fig.1. Within the studied field located in the Western area of Abu Dhabi (Fig.1), the basinal facies of this formation is the time equivalent of the progradational shelf margin facies of Mishrif Formation (Al-Zaabi et al. 2010). It is composed of nearly pure limestones with very little siliciclastics and shale (Makarychev et al., 2018). In UAE, this formation is a source rock for Mishrif and younger Cretaceous formations. It has the maximum subsurface thickness in the areas where Mishrif Formation is not present, with non-eroded thickness ranging between 500 ft to 900 ft from the deep basin to the slope, respectively (Taher, 2010 and Van Laer et al., 2019).

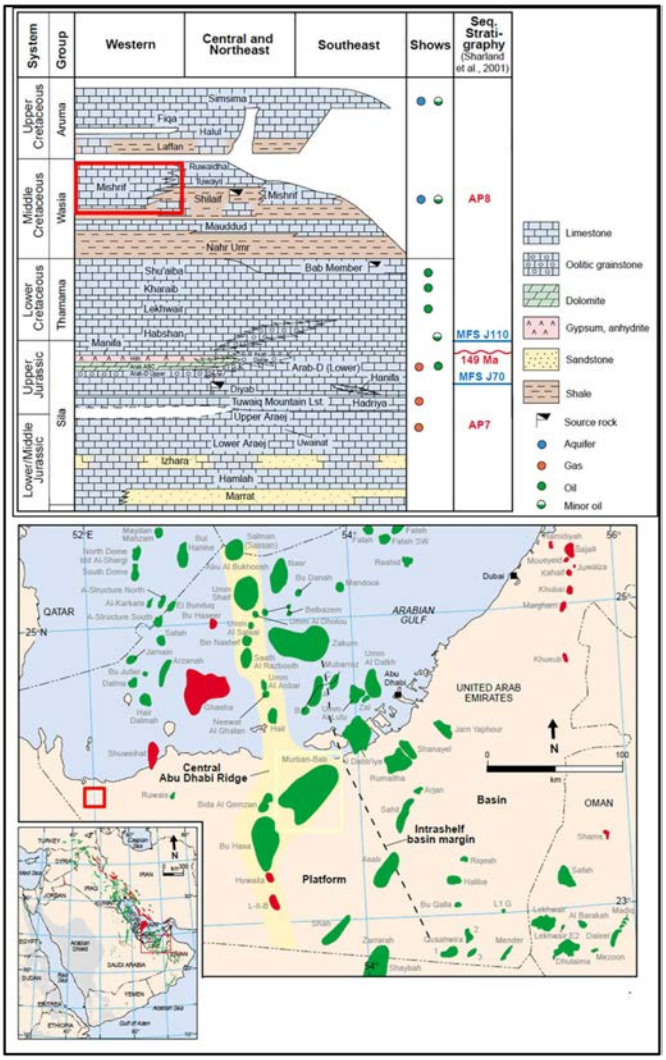

Figure 1—The Stratigraphic column of UAE (top) and location map of the area of study (bottom) (Modified after Grotsch et al., 2003). The studied formation and the field location are labeled by a red rectangle.

Previous conventional core analysis studies indicate that Shilaif Formation is principally a dark, bituminous, fine-grained wackestone to packstone rock, rich in planktonic foraminifera, with a Type I and Type II source rock, mainly within the immature to early oil-generation windows. TOC measures have ranged between 0.03 to 5 wt.%, with some local estimations reaching up to 15% (Taher, 2010; Al-Zaabi, 2010 and Tian 2019).

Reported porosity values moved between 2% to 5% (Van Laer et al. 2019, Steiner and Ahsan et al., 2015), going up to 10% in lean organic intervals (Bhatt et al., 2018), while the permeability was in the 30 nD to 300 nD range (Steiner, 2015 and Raina et al., 2015).

Historically, the volatile oil prices, in addition to the high production costs associated with the unconventional plays, have posed a high-economical risk for both National and International oil companies. Hence, improper rock characterization of non-conventional reservoirs can severely impact the finances and investment plans of ADNOC. Thus, the enhancement of commonly used characterization workflows in unconventional studies is essential for examining and identifying prospective hydrocarbon intervals and evaluating its real productivity potentials.

In this paper, the Cenomanian deposits of Shilaif Formation were studied using a comprehensive and integrative conventional and digital core analysis workflow designed to characterize its geological, geochemical, and petrophysical aspects and understand its hydrocarbon quality and production potentiality.

Methodology

One-hundred feet of continuous whole-core were characterized from the Shilaif Formation in west Abu Dhabi. The workflow comprised four main analytical stages, as shown in Fig. 2: Core Characterization using X-ray Dual Energy Scanning and Spectral Core Gamma (SCG), Geochemical and Petrophysical Characterization using physical methods, pore Characterization using 2D SEM Analysis, and properties upscaling and integration with the wireline logs.

Initially, the core X-ray DE CT scanning, a technique that has proved its ability in identifying the sweet spots within the unconventional source rocks (Walls et al. 2012), produced bulk density (BD) and photoelectric factor (PE) logs and gray-scale CT images at a resolution of 0.5 mm/voxel. These logs were integrated with the SCG logs to estimate porosity, organic matter content, brittleness index, and mineral composition and to define CT machine learning rock types (CT RTML Facies) by clustering all the DE CT-derived parameters using machine learning algorithms. The resulting logs were subsequently integrated with wireline logs to calibrate them, identify the locations of sweet spots along the core length, and extract representative plug samples for characterization purposes.

In stage two, petrophysical lab tests such as mercury injection capillary pressure (MICP), nuclear magnetic resonance (NMR), and crushed rock analysis (CRA) were performed. They provided critical petrophysical properties represented by porosity, gas permeability, fluid saturations, pore throat size diameters, essential parameters to understand the flow properties of Shilaif source rock. Additionally, geochemical analyses, including LECO TOC, HAWK, vitrinite reflectance, liquid chromatography (SARA), XRD, and XRF tests), were also conducted. These tests helped determine the OM content, hydrocarbon thermal maturity, productivity and composition, and the mineral and the rock matrix elemental composition. These analyses are essential to evaluate the quality and hydrocarbon potentiality of the studied source rock.

Stage 3 aimed to characterize the rock at the pore scale by generating high-resolution 2D SEM images at a 10 nm/pixel resolution, segmented by separating the pores, organic matters, and mineral phase digitally. These segmented images allowed the determination of pore types and the estimation of total, effective, and organic matter associated porosities (PAOM) and organic matter content (TOC). These outputs enhanced the understanding of the flow behavior of these tight and complex rocks. The final stage (Stage 4 in Fig. 2) consisted of fully digital and conventional core analysis upscaling, integration with the wireline logs, and identifying the most prospective zones within the studied intervals for economical utilization.

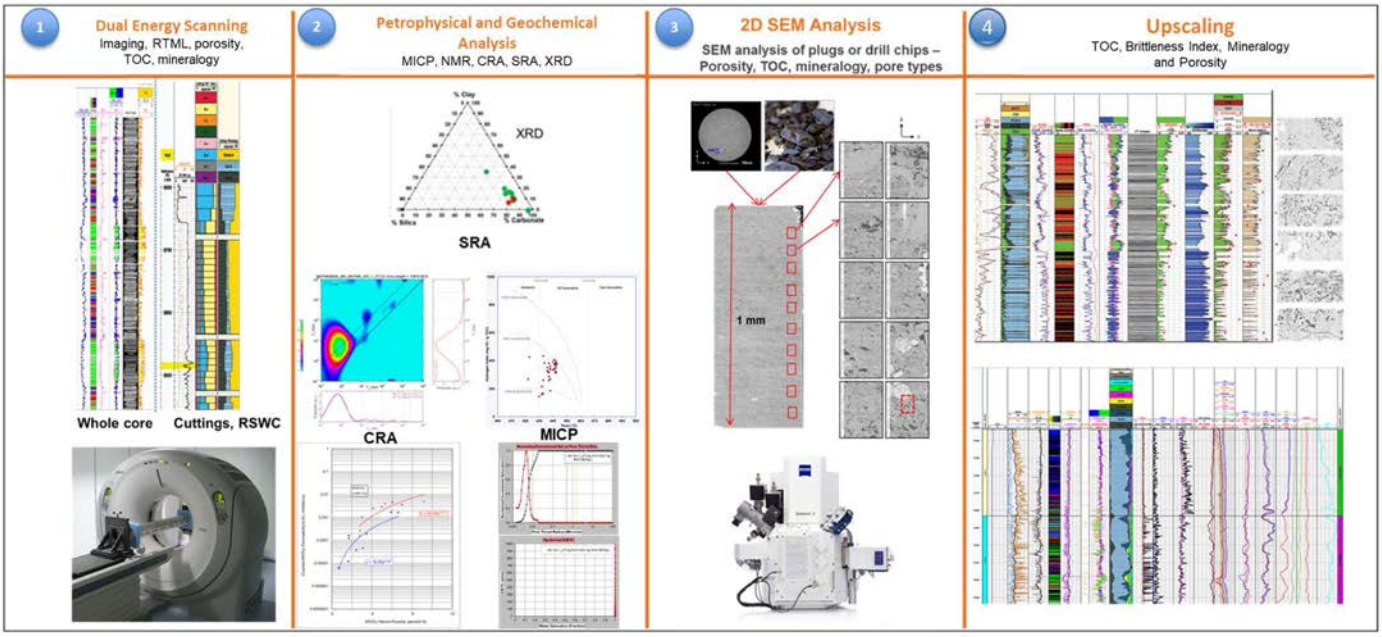

Figure 2—The workflow diagram shows the four stages of the characterization and integrative program implemented in this study. 1) The core characterization stage in which the X-ray DE CT scanning and SCG analysis were executed. 2) The petrophysical and geochemical stage in which several physical lab tests were implemented. 3) The pore characterization stage in which the 2D SEM imaging and digital segmentation were performed. 4) The upscaling stage in which the digital and conventional core analysis results were integrated with the wireline data.

The whole core characterization program was flexible in prioritizing some analyses, especially at the early stages of the drilling program, to assist in decision-making under the tight operational chronograms and the complex reservoir conditions.

Results and Discussion

Core Characterization and Identification of Potential Sweet Spots

The 4 inches diameter whole core was imaged using high-resolution X-Ray DE CT scanning to produce continuous bulk density (BD) and photoelectric factor (PE) logs, along with 3D core volumes and CT images.

Significant alterations in BD and PE logs and CT textures were observed by comparing the generated logs with the gray-scale CT images, exposing the high degree of heterogeneity of Shilaif Formation. For example, the top section of Shilaif from ×034 ft to ×084 ft is made mainly of tight, organic matter-poor and massive carbonate rock (mostly calcitic), as inferred in the gray-scale CT images and the BD-PE logs in Fig. 3a and the BD and PE cross-plot in Fig. 3b. On the other hand, the middle and bottom sections of Shilaif (×084 ft to ×134 ft) are made predominantly of alternating organic matter-rich (porous) and organic matter-depleted (tight) layers, of calcitic and argillaceous composition. The BD values logged in Shilaif cores vary considerably, probably because of porosity and organic matter content variabilities, ranging between 2.03 and 2.87 g/cc, with an average of 2.54 g/cc for the formation. On the contrary, the logged PE values fluctuate slightly, ranging between 3.35 and 5.75 barns/electron, with an average of 4.73 barns/electron, which is close to the calcite PE value of 5.06 barns/electron.

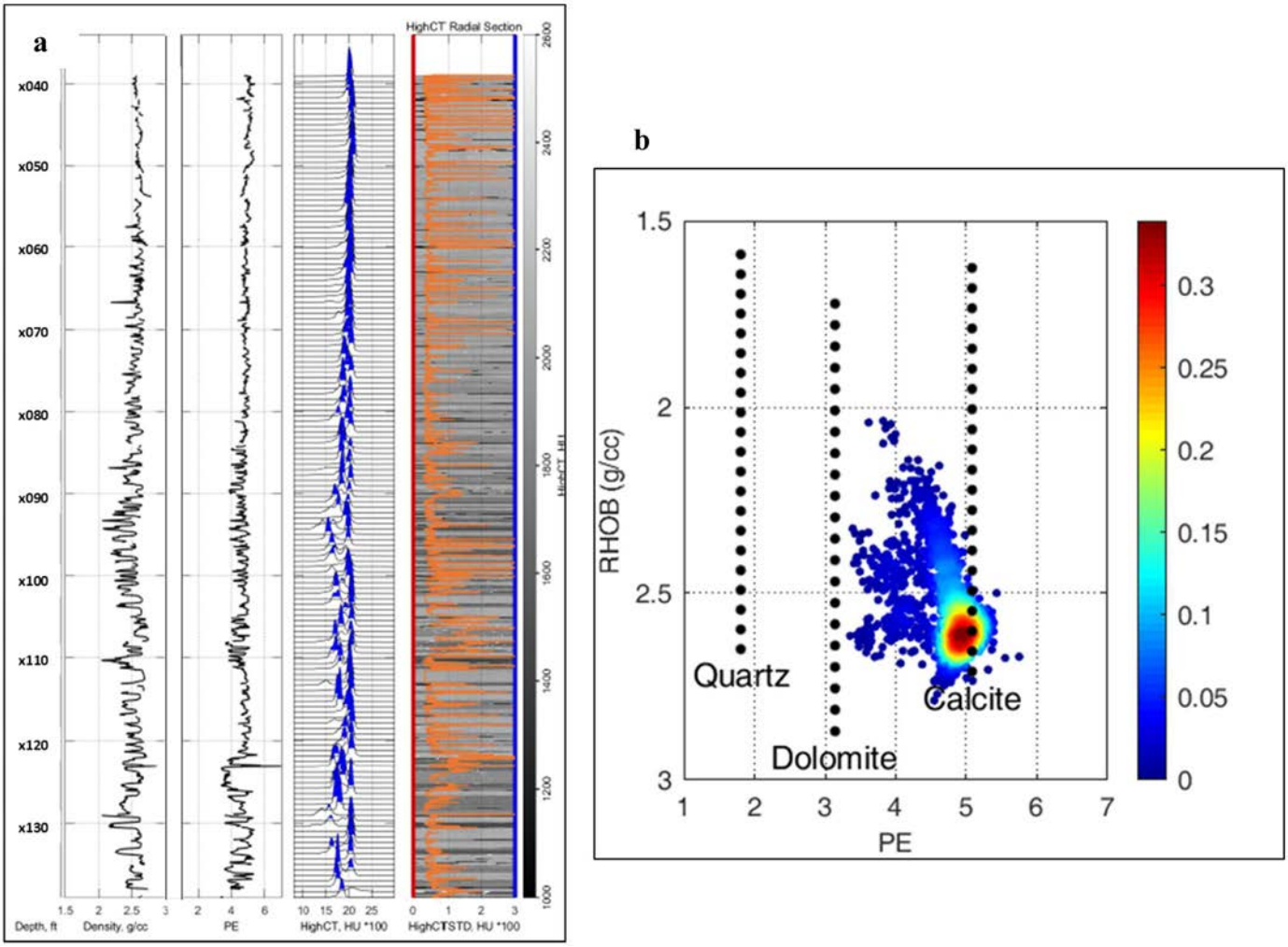

Figure 3—a) From right to left, the bulk density (BD), photoelectric factor (PE), High CT, and CT image logs derived from DE CT scanning. b) The DE derived BD and BE data population cross plot of the scanned Shilaif Formation cores.

The total Spectral Gamma Ray (SCG) logged on the surface showed a good match with the wireline-derived total gamma log, as shown in track 2 in Fig. 4, with high radioactivity, averaging 98.6 API, observed in the whole formation. The total gamma in the middle and bottom of the formation (red and blue rectangles in Fig 4), where hydrocarbon source rocks are expected, averaged 81 API. This relatively high radioactivity is attributed to the high concentration of uranium (34.8 ppm on average) in their rock-forming minerals (track 5 in Fig. 4). Based on Morton-Thompson et al., 1992, the high SCG radioactivity related to high U enrichment is usually associated with organic matter content.

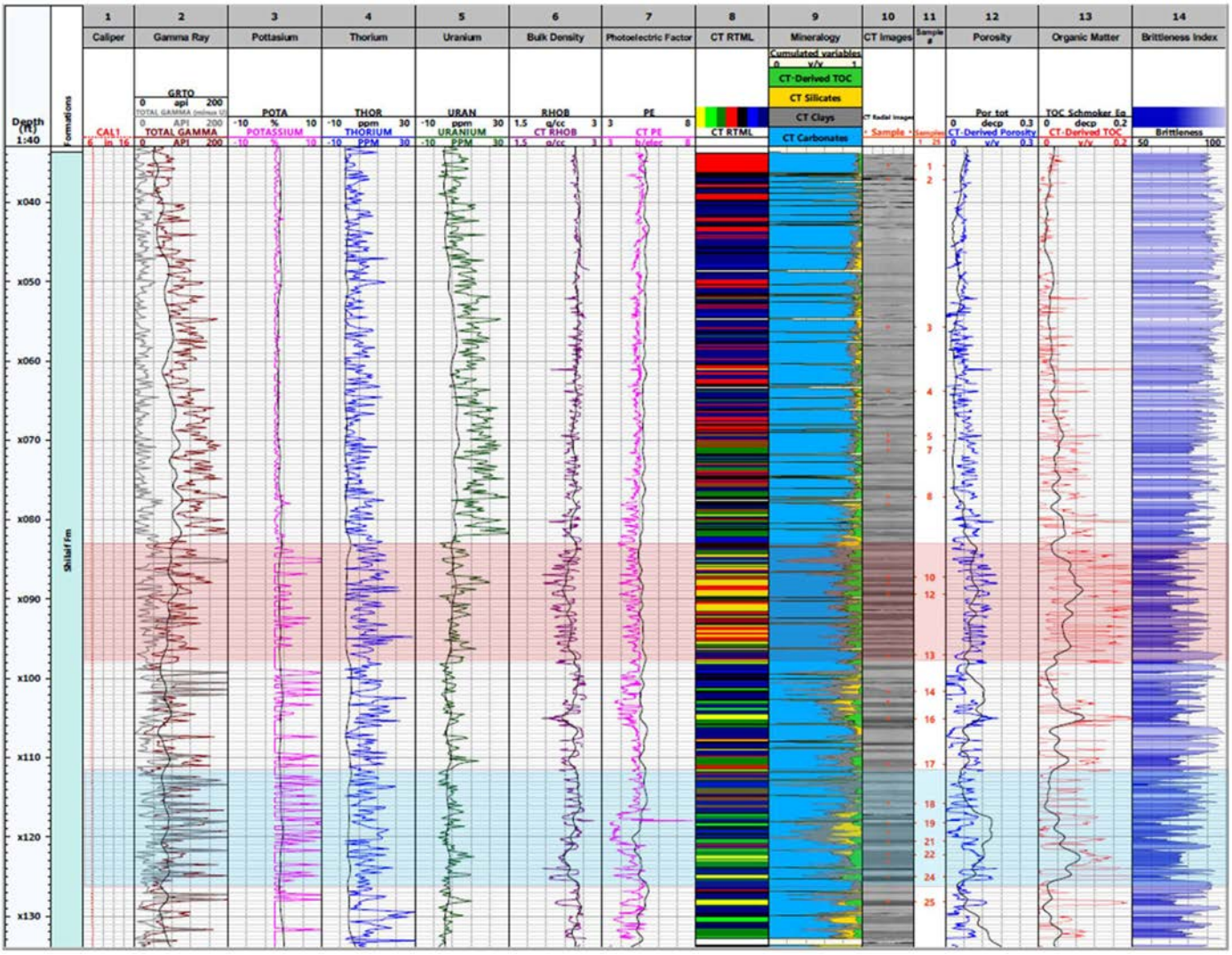

Figure 4—Integration log of DE CT derived data, spectral core gamma, and wireline data. The area highlighted in red seems to be prospective, given its high porosity (track 12), high organic matter content (track 13), and relatively high GR and uranium concentration (track 2). Tracks 10 and 11 show the selected sample locations for extraction and advanced core analysis.

Both DE CT data and Spectral Core Gamma measurements were used to estimate several petrophysical aspects of the Shiliaf Formation using various petrophysical models. Accordingly, additional high-resolution porosity, organic matter content, brittleness index, and mineralogical composition logs were generated and upscaled to the core level at a 0.05 feet resolution. The TOC and porosity logs illustrated in tracks 12 and 13 in Fig.4 exhibit good correspondence with the wireline derived logs, showing that the middle and bottom sections of Shilaif (from ×084 ft to ×134 ft) and both identified zones (red and blue rectangles in Fig. 4) are relatively rich in organic matter and porosity, as it is also inferred from both SCG and DE logs.

On the other hand, the brittleness index logs showed the rock has transformed from highly brittle within the top of the formation (xx20 ft- xx50 ft) to intermediate, low brittle in the middle and bottom of the formation. This decrease in the brittleness index is usually attributed to the occurrence of organic matter, clay minerals, or both (Dernaika et al., 2017). Both components occur in the bottom of Shilaif as noticed from the normalized and upscaled clay, silicate, and carbonate mineralogy logs in Fig.4 (Track 9).

Furthermore, a machine learning algorithm was also used to identify the CT-derived machine learning rock-types (CT RTML). Accordingly, the rock is classified into seven CT RTML's (track 8 in Fig. 4), namely

RTML 1: yellow, RTML2: Green, RTML3: Dark Green, RTML4: Red, RTML 5: Black, RTML 6: Light Blue, and RTML 7: Dark Blue.

To understand the connotation of every CT RTML, the box logs in Fig. 5 include OM content, porosity, and mineralogy data for comparison purposes, with the CT PE vs. CT BD cross-plot displaying their distribution. The highest content of OM is observed in RTML's 1, 2, and 3, with a maximum of 0.32 v/v. The OM concentration decreases in RTML's 4 and 5 and is almost null in RTML's 6 and 7. The CT porosity averages 6.5% in the formation, with a maximum porosity of 17% noticed in the RTML1. Compositionally, the formation is mainly made of carbonates, with a significant presence of clays and silicates in RTML's 2 and 6.

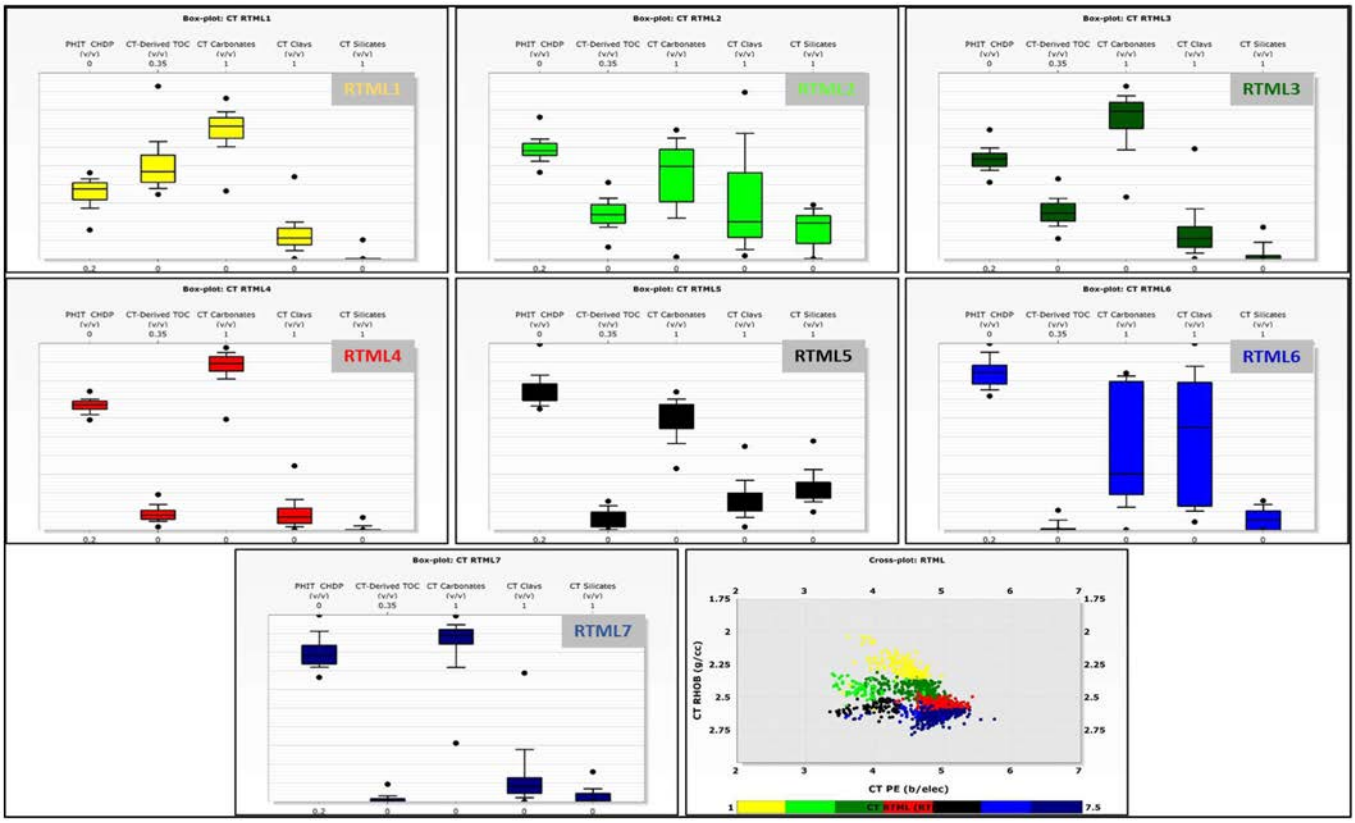

Figure 5—Box-logs illustrate the seven identified CT RTML and their properties in terms of porosity, TOC, and mineralogy (carbonate, clays, and silicates). The PE and BD cross plot on the bottom right shows the CT RTML facies and their domain within Shilaif formation.

The integration of DE CT and spectral core gamma data with wireline logs validated the core measurements and indicated the prospective locations to select and extract samples. Accordingly, twenty-five representative and well-distributed core plug samples were selected to cover all the geological and petrophysical variations in RTML's of Shilaif cores, as shown in the PE and BD cross-plot in Fig. 6.

Sample#	CT RTML	DE Rhob	DE PE
		g/cc	b/elec
1	4	2.56	5.14
2	7	2.61	4.95
3	7	2.61	4.83
4	3	2.39	4.63
5	1	2.35	4.67
6	4	2.54	4.86
7	3	2.46	4.77
8	3	2.45	4.78
9	5	2.59	4.10
10	4	2.52	4.98
11	1	2.06	3.86
12	1	2.22	3.91
13	7	2.65	5.00
14	5	2.54	4.22
15	2	2.43	3.68
16	1	2.21	4.44
17	3	2.39	4.75
18	7	2.66	5.00
19	2	2.40	3.44
20	6	2.64	3.62
21	3	2.40	3.87
22	3	2.38	4.20
23	1	2.35	4.45
24	1	2.16	4.11
25	1	2.29	4.32

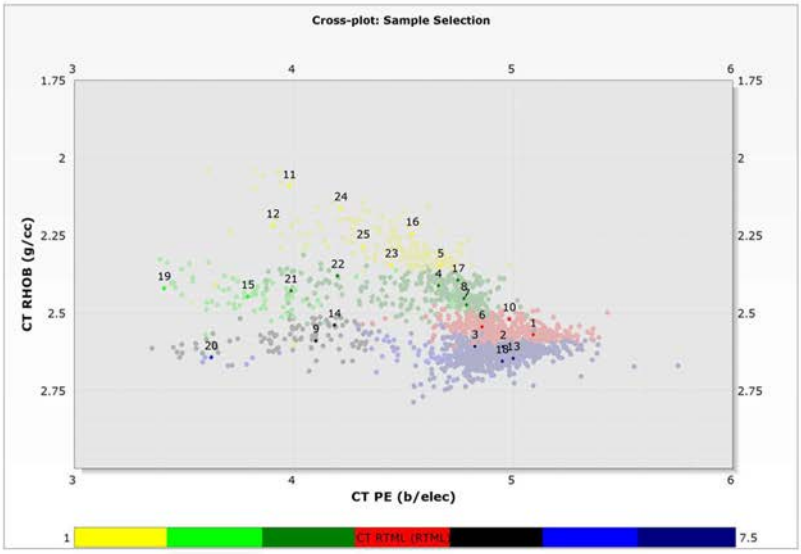

Figure 6—Left: the list of plugs samples extracted from the core with their corresponding BD, PE, and CT RTML Facies. Right: a BD vs PE cross plot displaying the samples selected from each CT RTML within Shilaif Formation.

Petrophysical Characterization

Twenty-five samples selected and extracted from Shilaif cores were characterized petrophysicaly using three different analytical methods; Mercury Injection Capillary Pressure (MICP), Crushed Rock Analysis (CRA), and NMR.

Mercury Injection Capillary Pressure (MICP)

Before running the MICP tests, the porosity of the analyzed samples was measured using the helium porosimeter. The measurements showed a low average porosity of 2.4%, with a maximum of 5.3%. The MICP analysis yielded low porosity measurement, which compared well with the He porosity results with an average of 2.3% and a maximum value of 5.2%. Similarly, the estimated Hg derived permeability is very low, with an average of 0.00051 mD. This low permeability and porosity reflect the tightness of this source rock as inferred from the Hg porosity and permeability cross-plot shown in Fig. 7a.

As for the pore systems, the MICP derived pore throat size distribution (PTSD) curves illustrated in Fig. 7b unveiled a micro to nanopores structure with a pore throat radius smaller than 0.1 microns in all the samples (Fig. 7b). Moreover, some samples have a pore throat radius smaller than 0.01 microns, with bimodal PTSD at the macro and nanoscale, as featured in the PTSD curves colored by red in Fig. 7b. Conversely, a few samples showed unimodal PTSD (green curves in Fig 7b). It indicates that Shilaif is heterogeneous not only at the macro and micro-scale but also at the nanoscale. The high entry pressure of the water saturations vs. Oil / Brine Capillary Pressure (Pc) drainage curves and its steep inclination, demonstrated in Fig. 7c, confirmed the complexity and low connectivity of the micro and nanopores within Shilaif Formation.

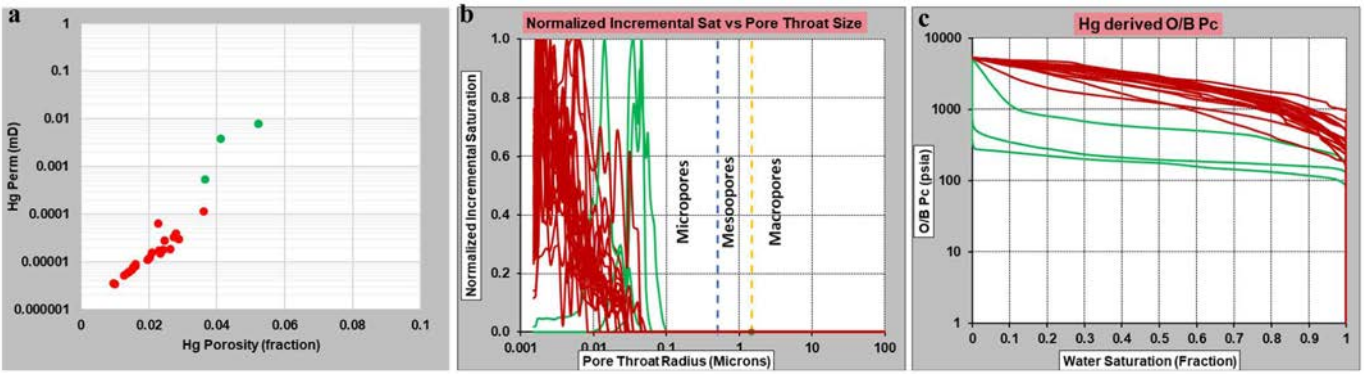

Figure 7—The outcomes of MICP Analysis. From left to right: a) pore-throat size distribution curves. b) Oil/Brine capillary pressure curves. c) Hg derived Porosity-Permeability cross plot for 25 plug samples.

Nuclear Magnetic Resonance (NMR)

The T1 and T2 relaxation time response from NMR analysis was carried out on 21 samples at three different conditions: as received (before fluid extraction), dry (after fluid extraction), and 100% brine saturation. The distribution and relation between these relaxation times helped understand and determine the type of hosted fluids and pores.

NMR porosity (Fig. 8), predicted from adding fluid-filled porosities with bitumen, averaged 3.17 p.u. for the AR condition, 1.18 p.u. for the dry state and 4.63 p.u. for the brine-saturated condition. In this prediction, the fluid-filled porosity refers to the summation of fluids in inter-particle pores, hydrocarbon in OM pores, and bound water. As per the fluid in the interparticle porosity log illustrated in Fig.8, this type of pores are common in the top of the formation (×034-x084), as confirmed through the 2D SEM images obtained for the samples derived from the Top Shilaif (Sample 3 Fig. 13), while they are rare towards the mid and bottom Shilaif Formation (×084 ft to ×134 ft). Pores hosted within the organic matter are dominant at the middle and bottom of Shilaif, as indicated from the As received HC in OM log illustrated in Fig. 8 and the 2D SEM image of sample 10 in Fig 13. The CBW porosity is very low in Shilaif formation except in the clay minerals rich intervals (between ×104 and ×128 ft), as observed from the upscaled mineralogy logs in Fig. 5 and the 2D SEM image of sample 25 in Fig 13.

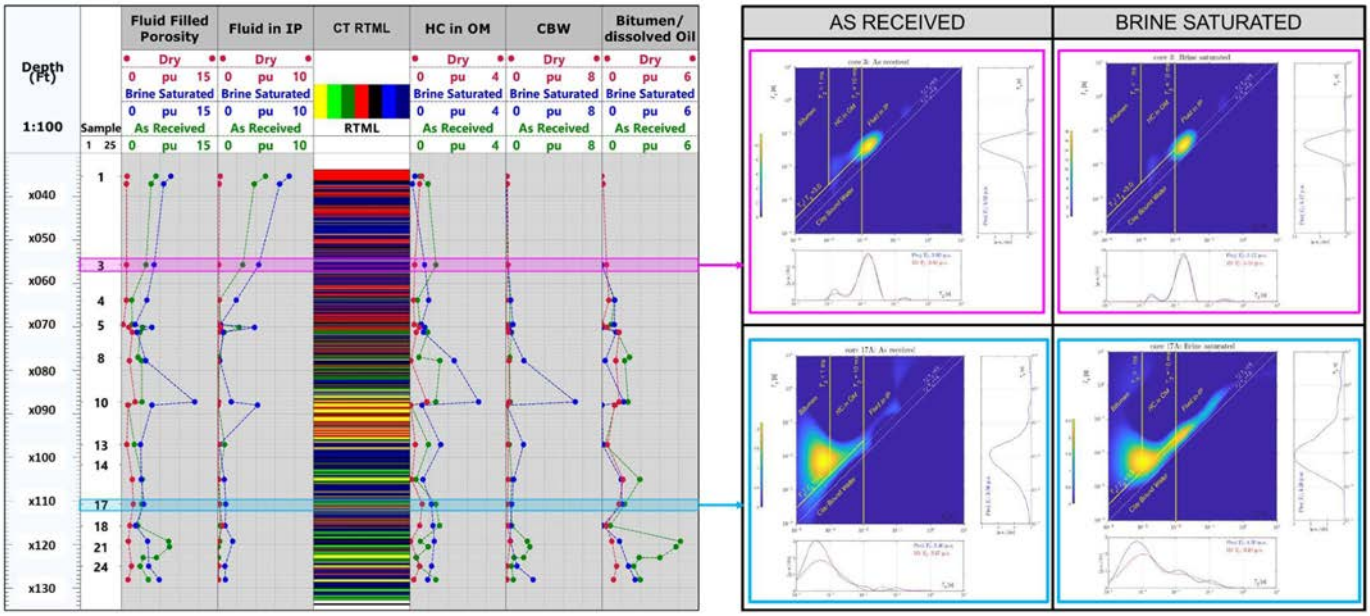

Figure 8—NMR porosity partition data for 21 samples, at three different stages, is displayed in the log on the left. The T1-T2 maps on the right show the fluids distribution for a sample with predominately intraparticle porosity (top maps outlined in pink) and an organic-rich sample (bottom maps outlined in blue).

The classification of these fluid-filled regions and the bitumen in the T1-T2 maps shown in Fig. 7 was determined from establishing T1-T2 distribution and T1 / T2 ratio cutoffs, similar to the T1-T2 relaxation distribution proposed by Kausik et al., 2015. A T2 signal of 1 ms and a T1 / T2 ratio above three was attributed to bitumen/dissolved oil. A signal above a T2 of 1 ms and a T1 / T2 ratio equal to three was assigned to oil in OM. A T2 signal above of 1 ms and under T1 / T2 ratio of 3 corresponded to bound water. Finally, a signal above T2 of 10 ms was allotted to fluid in inter-particle pores.

The relatively high occurrence of the organic matter and hydrocarbons in the mid and bottom of Shilaif can be deduced from the very fast-relaxing time, as shown in the corresponding T1-T2 map of sample 17 and the Bitumen/dissolved oil log in Fig.8. The opposite occurs in the low organic matter content samples derived from the top of Shilaif that have a dominant signal at around 20-40 ms, which falls in the interparticle porosity region.

Crushed Rock Analysis (CRA)

The determination of porosity, permeability, and fluid saturations were obtained from the CRA measurements under the as received (AR) and retorting and dry (after extraction) conditions. The CRA data showed that the total AR saturations for brine, oil, and gas within Shilaif averaged 2.51%, 1.50%, and 0.77% of the bulk volume, respectively. This estimated average brine saturation comprises 1.44% Vb Clay Bound Water and 1.07% Vb Free Water. The oil is more abundant towards the mid and bottom of Shilaif with a maximum saturation of 4.8 % Vb, as shown in the AR oil saturation log in Fig. 9, which aligns with the NMR analysis findings. On the other hand, the gas saturation is low and its saturation is not varying remarkably along the core length with the highest saturation of 2.5% Vb as shown in the AR gas saturation log in Fig. 9. The average AR Press-Decay Permeability of Shilaif is 0.000025 mD with an average as received porosity of 4.78% along the core length, as illustrated in the AR porosity and permeability log in Fig.9. These very low porosity and permeability values are clear evidence of the poor quality of the rock in petrophysical terms.

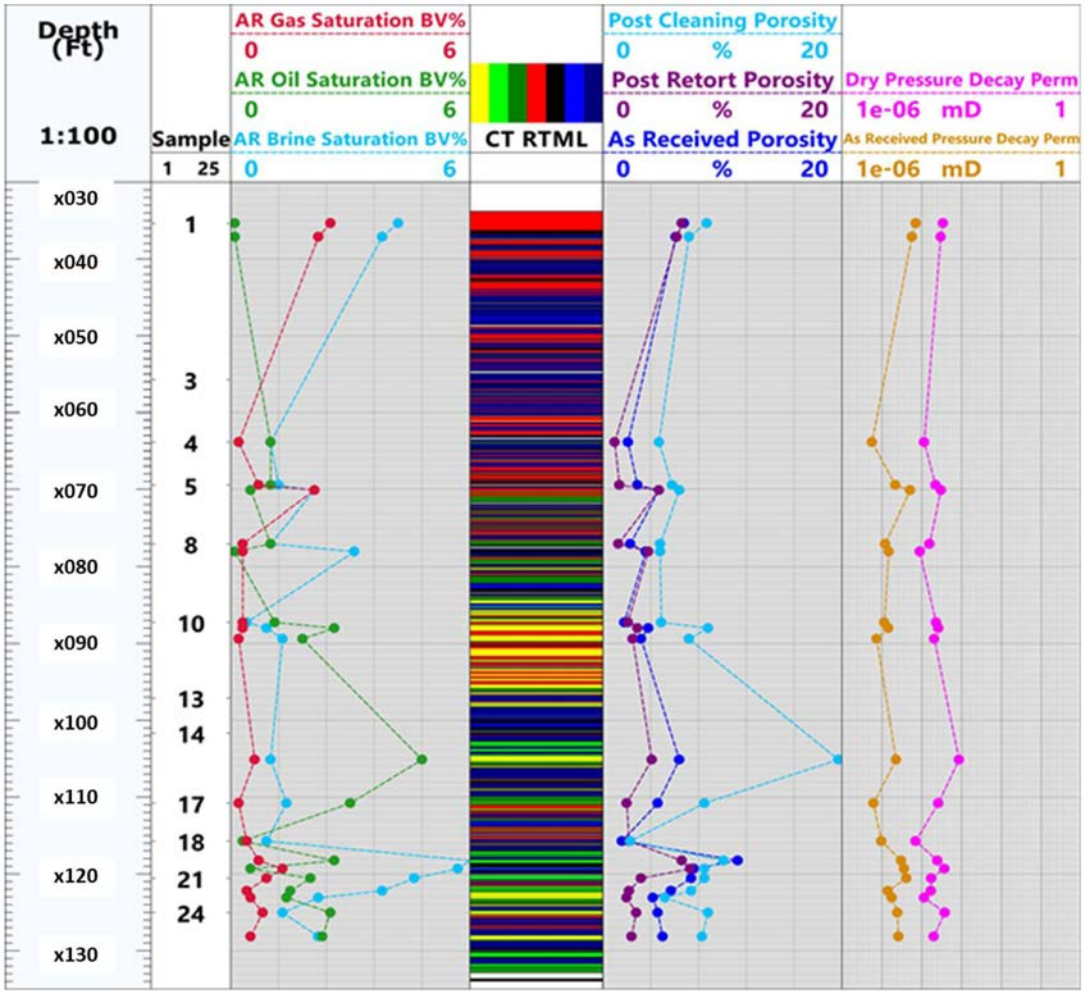

Figure 9—Crushed rock analysis log showing saturation, porosity, and pressure-decay permeability data for 25 samples and its relation with the CT RTML Facies.

Interestingly, after the extraction of the oil and drying of the samples, the porosity and permeability have increased to 7.52% and 0.00025 mD, respectively, especially towards the mid and bottom of Shilaif, as shown in the post-cleaning porosity and dry pressure decay permeability logs in Fig.9. This can be attributed to the extraction of the dominant oil from the pore structure of the analyzed samples during the retorting and extraction processes. These CRA-derived porosities and permeabilities are consistent with the ones obtained from MICP and NRM, which reflect the tight nature of this source rock.

Geochemical Characterization

X-ray Diffraction (XRD), LECO TOC, HAWK pyrolysis, vitrinite reflectance, and liquid chromatography analysis (SARA) were carried out to characterize the geochemical features of Shilaif Formation

LECO TOC and HAWK Analysis

Both the organic carbon quantification and thermal maturity assessment are indispensable parameters in evaluating the unconventional source rock (Steiner et al., 2015). The LECO TOC measured for the 25 samples showed low OM content (poor potential) in the top of Shilaif (×034 ft- ×084 ft) and good OM content (excellent potential) towards the mid and bottom of Shilaif with an average of 4.78 wt% as illustrated in the LECO TOC log in Fig. 10. This TOC content is in line with the upscaled TOC log derived from the integration between the DE CT scanning and SCG in Fig. 5.

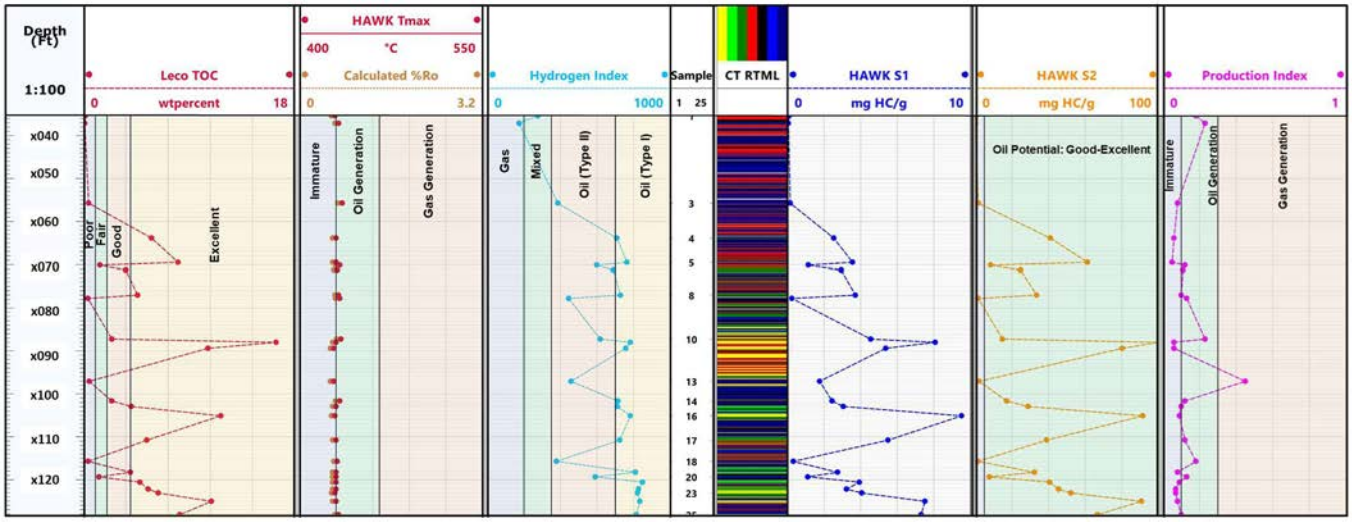

Figure 10—From left to right: the measured LECO TOC to deduce the source rock potential; Tmax and Calculated Ro %, which define the thermal maturity of the hosted organic matters; calculated Hydrogen Index (HI) log that is used to determine the kerogen type; analyzed samples locations; Shilaif identified CT RTML Facies; measured S_1 index of the analyzed samples which relates to the free hydrocarbon or movable oil; the measured S_2 index which reflects the oil potential; The calculated Production Index (PI) which reflects the maturity level of the hosted organic matters.

The HAWK pyrolysis showed that the S_2 index (oil potential) is averaging at 36.52 mg HC/g and reaching up to 128.22 mg HC/g, as shown in the S_2 log of Fig. 10. The free hydrocarbons or producible oil inferred from S_1 index is averaged 3.39 mg HC/g, with a maximum value of 9.51 wt%. These values indicate a Poor to Fair free oil source, as observed from the S_1 log in Fig.10. S_1 and S_2 values increase towards the mid and bottom of Shilaif, indicating good hydrocarbon potential as had been inferred earlier from NMR and CRA results.

The production index (PI) was calculated by dividing S_1 index over the summation of S_1 and S_2 indices. The computed values showed that the top of Shilaif is immature while its mid and bottom areas fall within the early oil generation window with an average PI of 0.12 (PI log in Fig.10). The average maximum temperature (Tmax) measured from pyrolysis is equal to 431°C (Tmax log in Fig 10).

The vitrinite reflectance (Ro%) calculated from the Jarvie, et al., 2001 equation (%Ro = 0.018 * Tmax − 7.16) averaged 0.59 %Ro in the formation. This value suggests that the organic matter of Shilaif, especially at the top of the formation, falls within the immature window, demarcated at 430 °C and 0.6 Ro%, with a few samples, mostly in the mid and bottom of Shilaif, falling within the oil generation region (the calculated Ro% track in Fig.10). The hydrogen index calculated by the (HI= (100 × S_2) /TOC) equation, averages 649 in the whole formation, denoting that most organic matter has kerogen type II of marine origin (Tissot and Welte, 1984; Peters and Cassa, 1994).

Liquid Chromatography-SARA (Saturate, Aromatic, Resin, and Asphaltene)

The determination of hydrocarbon fractional composition in crude oils is fundamental to assess possible production problems related to asphaltene components and the abundance of saturate and aromatic hydrocarbons (Fan et al., 2002). In SARA analysis, the saturate fraction consists of nonpolar material, including linear, branched, and cyclic saturated hydrocarbons. The Aromatics, with one or more aromatic rings, are more polarizable, while the resins and asphaltenes have polar substituents (Fan et al., 2002).

SARA analysis has been done on a total of 20 samples of Shilaif Formation. The result showed that the hosted crude oil in this formation is made mainly of Aromatics (46wt % on average) followed by resin (30wt % on average), especially in the mid and bottom of the formation, as illustrated in the pie chart in Fig. 11. The saturate is the third most common component in Shilaif crude oil with an average of 14 wt%, especially towards the bottom of Shilaif. The asphaltenes have the lowest concentration in the crude oil of

Shilaif, with an average of 10 wt%, and a maximum concentration of 24.9 wt% displayed at the top of the formation. Based on the table in Fig.11, it is noticed that the saturate and asphaltene concentrations fluctuate significantly along the core length compared to the aromatics and resin components. Also, the extractable organic matter (EOM) of the middle and bottom intervals (11619.12 ppm on average) is higher than the top of Shilaif (4638.01 ppm on average), proving the potentiality of these units, especially the middle one.

Depth (ft)	SampleID	Saturates (wt%)	Aromatics (wt%)	Resines (wt%)	Asphalthene (wt%)	Sat / Aro	EOM (ppm)
XX35.33	1	13.64	22.73	59.09	4.55	0.60	139.50
XX37.13	2	23.08	7.69	53.85	15.38	3.00	45.71
XX63.87	4	7.32	49.12	18.65	24.90	0.15	6778.73
XX69.46	5	6.62	43.00	30.03	20.36	0.15	8322.95
XX70.08	6	9.27	43.74	30.45	16.54	0.21	3673.09
XX77.00	8	7.26	47.85	31.68	13.20	0.15	12698.79
XX77.76	9	12.32	43.48	37.68	6.52	0.28	807.28
XX87.24	10	10.70	53.51	21.52	14.27	0.20	16655.82
XX87.99	11	6.05	48.68	28.06	17.21	0.12	16716.45
XX89.37	12	5.37	47.87	32.21	14.54	0.11	11407.95
X105.10	16	8.58	52.42	25.59	13.42	0.16	21580.42
X110.79	17	14.75	53.26	22.67	9.32	0.28	10983.82
X115.72	18	23.89	48.33	25.56	2.22	0.49	1181.45
X118.23	19	21.71	53.29	23.46	1.54	0.41	9111.07
X119.28	20	26.49	49.88	22.20	1.43	0.53	2544.69
X120.56	21	22.51	49.76	25.59	2.13	0.45	10242.16
X122.17	22	13.50	49.31	33.88	3.31	0.27	9280.00
X123.07	23	12.08	50.28	30.06	7.58	0.24	7659.37
X125.01	24	11.41	48.55	26.37	13.67	0.24	17882.27
X128.14	25	20.80	48.54	24.82	5.84	0.43	15803.11
Average		*13.87*	*45.57*	*30.17*	*10.40*	*0.42*	*9175.73*

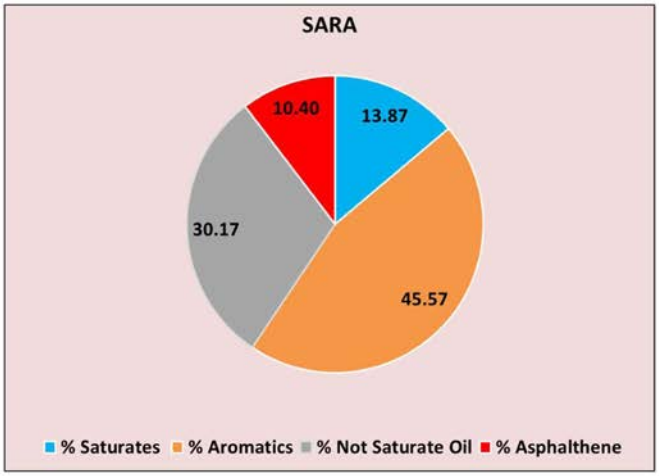

Figure 11—Left: a table summarizes Shilaif extracted crude oil composition obtained from SARA analysis for 20 samples. Right: a pie chart illustrates the composition of Shilaif crude oil.

Measured Vitrinite Reflectance

Vitrinite reflectance measurements were performed on ten samples (Fig 12a). The average measured reflectance in Shilaif equals 0.58 Ro% with a maximum measured value of 0.66 Ro%, which is an indication that Shilaif organic matter is marginal to early thermally mature and fall within the early oil generation window. Additionally, the Vitrinite Reflectance Equivalent (VRE) was calculated using Jacob, 1999 (VRE=0.618*SB+0.4), and Schoenherr et al. 2007 (VRE= (SB+0.2443)/1.0495) equations, which depend on the reflectance of the common and distinct solid bitumen (SB); the average calculated VRE using both methods is equal to 0.66% and 0.64%, respectively. These measured Ro% and VRE values confirm the early thermal maturity of the Shilaif hosted organic matter. They are in line with the calculated Ro% derived from HAWK analysis, which showed an immature to early thermal mature source rock.

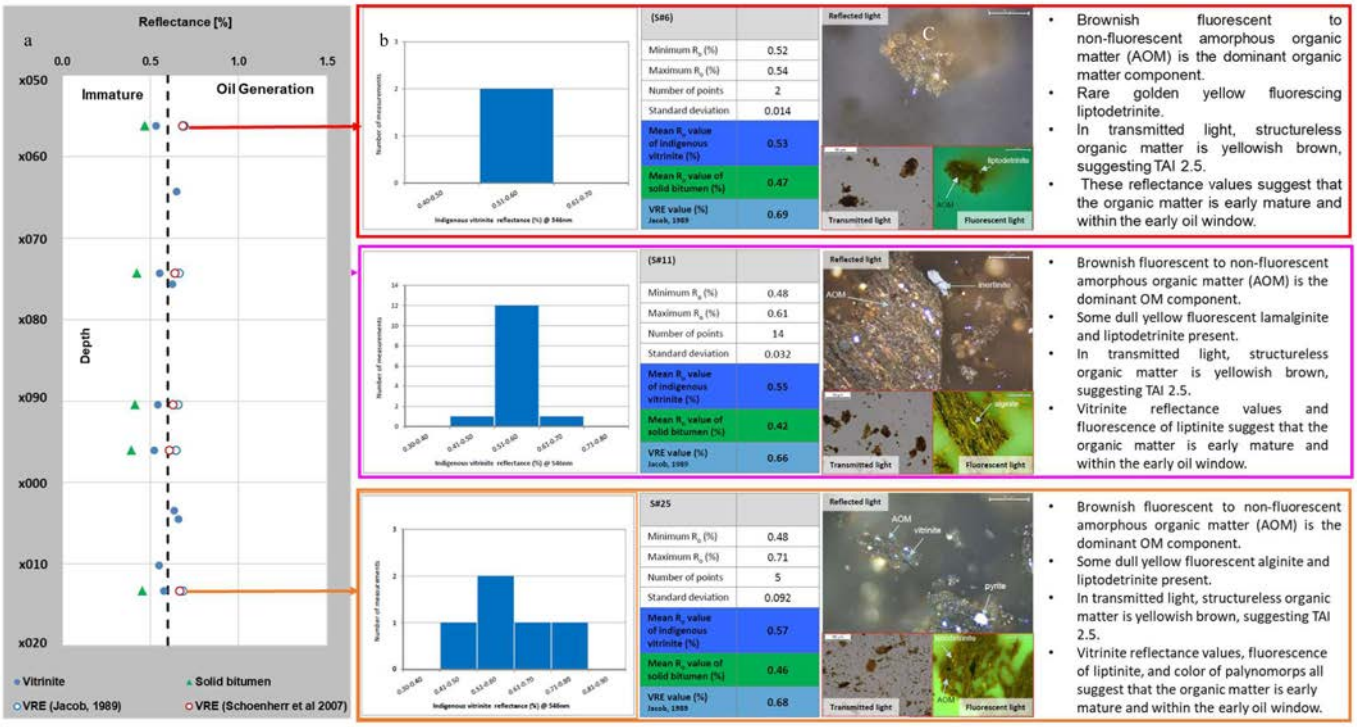

Figure 12—Vitrinite reflectance analysis for the ten analyzed samples from Shilaif. a) The log on the left shows the distribution fo the measured Ro% and calculated REV's for all analyzed samples. b) The measured Ro% and REV's of samples 6, 11, and 25 are displayed in the statistical histograms and tables. c) The reflected, transmitted, and fluorescent lights photomicrographs of the three samples with a brief description.

The visual analysis was done for macerals and kerogen using the reflected light microscope. The statistical histograms and tables of Fig. 12b and the observed reflected and fluorescent lights photomicrographs illustrated in Fig. 12c showed that the brownish fluorescent to nonfluorescent amorphous organic matters (AOM's) are the dominant in Shilaif. Massive AOM has reflectance ranging from 0.25 to 0.28%. There is also some dull yellow fluorescent lamalginite and liptodetrinite present. Vitrinite is sporadic and very small (borderline for reflectance measurements), and Inertinite is patchy. Some solid bitumen (5.3 Vol.% on average) was also present.

In transmitted light, the structureless organic matter is yellowish-brown, suggesting the thermal alteration index of Staplin, 1969 (TAI) equal to 2.5. Pollen and spores are orange ambers and their color assesses vitrinite reflectance at ~0.65%. The fluorescence of liptinite and color of palynomorphs all suggest that the organic matter is early mature and within the early oil window.

X-Ray Diffraction (XRD)

The mineralogical composition for the 25 samples was determined using the X-ray Diffraction method. The results revealed that the rock is made mainly of calcite, which averages 86 wt% of the rock, followed by clays minerals (illite+mica and kaolinite) and quartz that averaged 5 wt% and 3 wt% wt, respectively (columnar and ternary plots in Fig. 13).

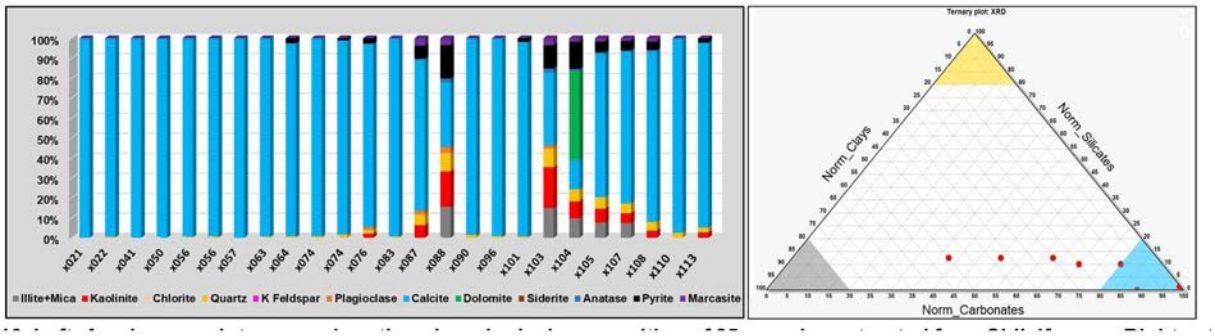

Figure 13—Left: A columnar plot summarizes the mineralogical composition of 25 samples extracted from Shilaif cores. Right: a ternary plot shows the mineral composition for 25 samples of Shilaif, normalized to three mineral groups: carbonates, clays, and silicates.

Calcite is the most dominant mineral at the top of Shilaif (98 wt. % on average), but its concentration decreased towards the bottom (74 wt. % on average). This concentration comes in line with the findings of the upscaled mineralogy log derived from DE CT and SGR logs illustrated in Fig. 4. The opposite was observed in the Mid and Bottom of Shilaif (×084 ft to ×134 ft), where both quartz and clay minerals concentrations increased relatively compared to the top part of the formation (the columnar plot in Fig.13)

Pyrite is abundant towards the bottom of the formation, reaching a maximum concentration of 16.7% wt and averaging 3.5 wt. % in all the samples. Some minerals like plagioclase, anastase, and marcasite occur but in a minor concentration. Only a single sample at depth (×104 ft) contains dolomite (40 wt. %).

Pore Analysis (2D SEM Analysis)

The challenge of quantifying and estimating petrophysical parameters in very tight pore systems hosted in source rocks in general and Shilaif in particular, where the micro and nanopore structures are controlling flow behavior (as shown in the MICP derived PTSD curves Fig.7), could be solved through the 2D SEM imaging workflow. Several researchers described this workflow before like Walls et al., 2011, Cantisano et al., 2013, Almarzooq et al., 2014, Moustafa et al., 2015 and Moustafa et al., 2017 in which advanced digital imaging and segmentation techniques were implemented to quantify porosities (effective, total, and associated with OM) and OM content parameters that are indispensable to evaluate unconventional source rocks.

The 2D SEM analysis showed that the total porosity of Shilaif is ranging from 0.08 vol.% to 9.39 vol.% with an average total porosity of 3.34 vol.%, while the average estimated effective porosity equals to 2.24 vol% (tracks 8 and 9 in Fig. 14). By comparing the wireline and upscaled CTderived porosity logs with the 2D SEM derived total and effective porosity, an acceptable match between them was noticed, especially at the top of the formation, where the HAWK-derived S_1 and OM content are very low (S_1 Log in Fig.10 and track 10 in Fig. 14). Sample# 3 in Fig.14 is an example of this case where the measured S_1 (0.15 (mg HC/g)) and estimated OM content (1.22 vol. %) are relatively low. The 10nm/pixel 2D SEM image of sample# 3 in Fig.14 showed that the interparticle (inorganic) pores are the most typical ones in this sample, confirming the findings of the NMR analysis (Fig.8).

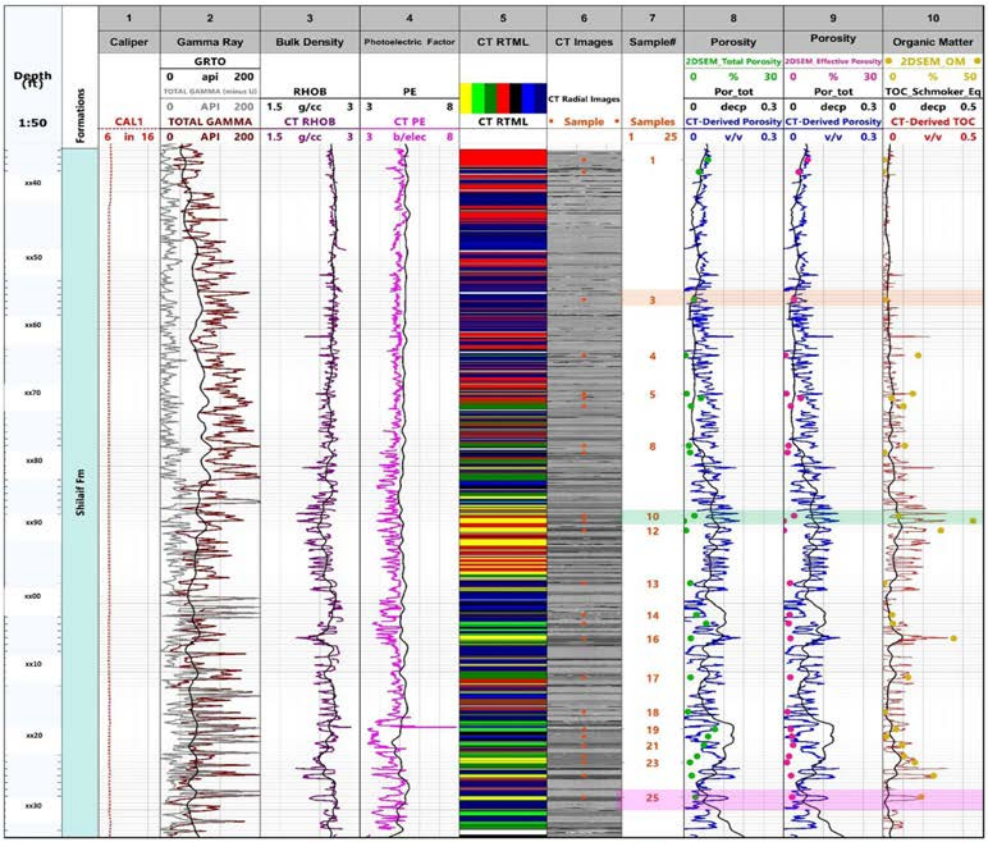

SAMPLE 3	
2D SEM Total Porosity (vol%)	3.08
2D SEM Effective Porosity (vol%)	3.08
2D SEM Organic Matter (vol%)	1.22
2D SEM Porosity in OM (vol%)	0.11

SAMPLE 10	
2D SEM Total Porosity (vol%)	3.20
2D SEM Effective Porosity (vol%)	3.20
2D SEM Organic Matter (vol%)	7.75
2D SEM Porosity in OM (vol%)	2.43

SAMPLE 25	
2D SEM Total Porosity (vol%)	3.54
2D SEM Effective Porosity (vol%)	2.83
2D SEM Organic Matter (vol%)	19.09
2D SEM Porosity in OM (vol%)	1.52

Figure 14—Top: a log compares the 2D SEM data with the DE CT data and wireline logs (tracks 8, 9, and 10); the data in general shows good agreement. Middle: an example of the 10nm/pixel 2D SEM images acquired for samples 3, 10, and 25. In each image, the OM appears in dark grey, the pores appear in black and the grains appear in light gray. Bottom: the digital upscaled segmentation results of the 10 nm/pixel 2D SEM images summarized in tables.

On the other hand, the total and effective porosities in the Mid of Shilaif, where the OM content and moveable oil S_1 are relatively high (S_1 log in Fig. 10 and Log 10 in Fig.14), the CT-derived and wireline-derived logs showed a slight mismatch. This discrepancy is probably attributed to the presence of crude oil and non-moveable bitumen in the pore systems of the analyzed samples. Sample# 10 in Fig.14 is an example of this case where the measured S_1 (4.55 (mg HC/g)) and estimated OM content (7.75 vol. %) is relatively higher than sample# 3. The 10nm/pixel 2D SEM image of sample# 10 in Fig.14 illustrated that the pendular and spongy pores are the most common porosity associated with the OM. This type of porosity made 75% of the volume of the total and effective porosities hosted in this sample.

Even though the OM content derived from the10nm/pixel 2D SEM image and log (track 10 in Fig.14) of sample#25 (19.09 vol.%) is high, the volume of the pores associated with OM is lower than the Mid of Shilaif, which agrees with the findings of NMR analysis (Fig.8). Although the 2D SEM images and NMR data confirmed the occurrence of these porosities in the mid and bottom of Shilaif, they are relatively less abundant, especially towards its bottom, because of its low degree of transformation. The relatively higher concentration of clay minerals (mainly illite and kaolinite) in Mid and Bottom of Shilaif can be observed clearly from the 10 nm/voxel images of samples#10 and 25 in Fig.14 where they have a sheet-like appearance.

The CT and wireline derived TOC logs (Log 10 in Fig.14) with the 2D SEM estimated OM content (the yellow data point in Log 10, Fig.14) were compared, and a good match was achieved, with an average TOC content of 11.53 vol% (equivalent to ~5.77wt %) along the core length.

Core Analysis Results and Wireline Logs Integration

All the obtained conventional and digital core analysis results were integrated with the wireline logs for validation purposes, to understand the properties of Shilaif Formation better and determine its most prospective units. Fig. 15 displays this integration in which the wireline logs (colored in black in all the tracks) were combined with the core analysis results. The formation has been splitted into three zones to differentiate the most and least prospective areas in the core. The Zone 1 (highlighted in yellow in Fig 15), Zone 2 ((highlighted in red in Fig 15) Zone 3 (highlighted in blue in Fig 15), extend from ×034- ×084 ft, ×084- ×097 ft and ×103- ×129, respectively.

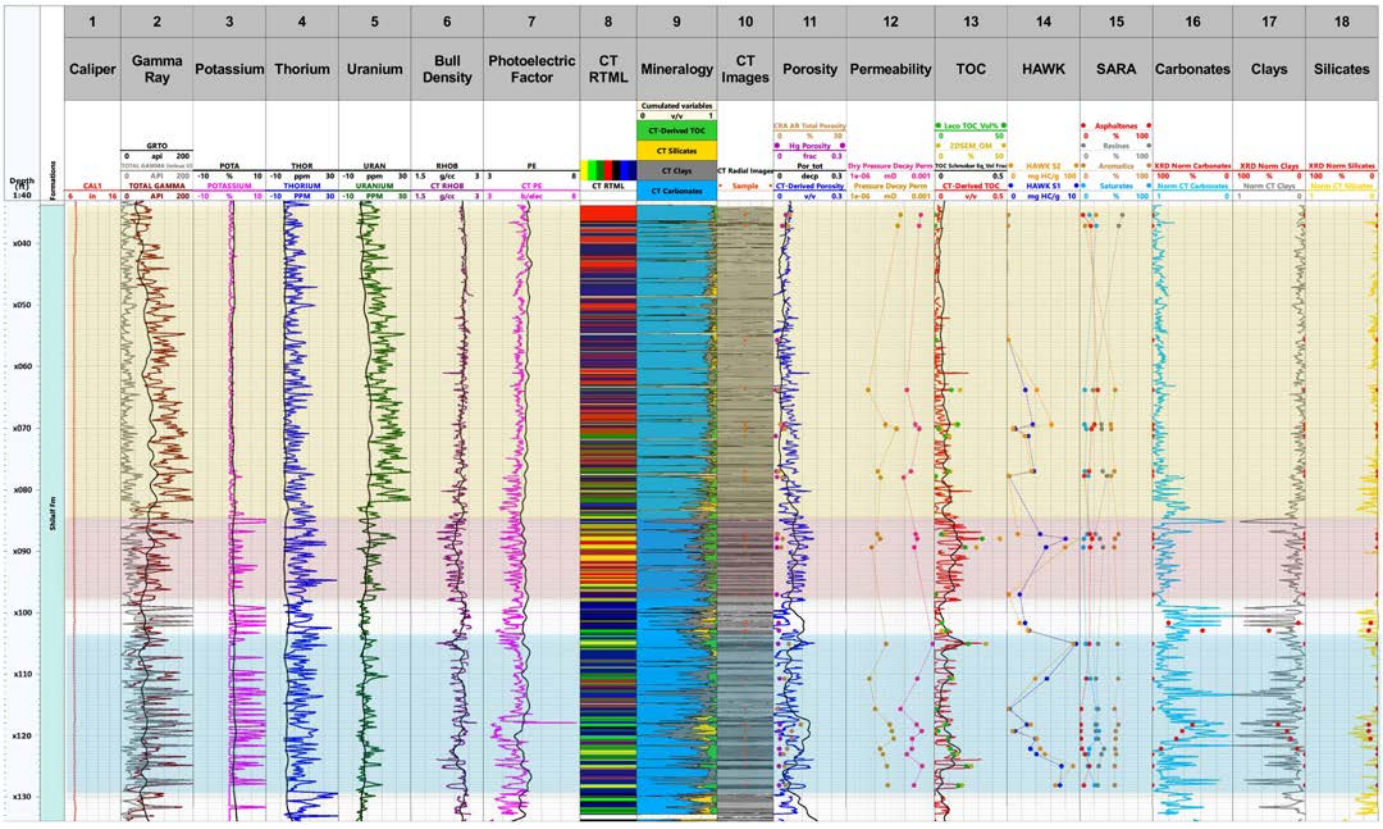

Figure 15—Integration log comparing data acquired from DE CT scanning, spectral core gamma, plug lab tests, and wireline logging. Three areas are differentiated in the reservoir based on petrophysical and geochemical data: the yellow area encloses the rock with the poorest quality reservoir. The red area represents the best quality reservoir. The blue corresponds and are with high potential, but affected by the presence of clays.

The Zone 1 is characterized by its tight nature with low porosity (0.06 v/v on average) and OM content (average of 0.024 v/v, equivalent to ~0.012 wt fraction) compared to the mid and bottom zones of Shilaif (Tracks 11 and 13 in Fig.15). The GR values are the highest for this formation because of the abundance of uranium element in the main rock-forming minerals (mainly calcite). This zone has poor hydrocarbon prospectivity.

The SCG derived logs (tracks 2, 3, and 5 in Fig.15) suggest two zones with high prospectivity. The first zone (Zone 2) in Mid of Shilaif was inferred from the high gamma radioactivity linked mainly to the occurrence of organic matters and clay minerals. The DE CT derived logs displayed in Fig. 15 from tracks 6 to 10 confirmed that this zone has the highest upscaled OM content in Shilaif (averaging 0.096 v/v, equivalent to ~0.048 wt fraction) and good upscaled porosity (average of 0.09 v/v) and is made mainly of carbonate minerals (mainly calcite), followed by minor concentrations of clay minerals and silicates (Tracks 16, 17 and 18 in Fig.15). The RTML facies (Track 8 in Fig.15) associated with this zone are one (Yellow), three (Dark green) and four (Red), which are characterized by relatively moderate OM content and porosities (track 9 Fig. 15) and reflect the potentiality of this zone.

Towards the bottom of the formation, another prospective zone (Zone 3) was identified. In this zone, the upscaled OM content averaged 0.038 v/v (equivalent to 0.019 wt fraction), with an average porosity of 1.7 v/v. Mineralogically, the SGR logs indicate the thorium and potassium elements are dominant in this zone, which is attributed to the occurrence of clay minerals and silicates. The upscaled mineralogy log in Fig.15 (Track 9) showed that Zone 3 is richer with clays and silicates than Zone 2. This observation has been proved from both the XRD analysis and 2D SEM images (Fig. 13 and 14, respectively). The most dominant CT RTML facies in Zone 3 are the RTML3 (Light Green) and RTML6 (Light Blue), which exhibit low to moderate organic matter content, moderate porosity, and relatively moderate to high clay richness.

The results of petrophysical testing run on different plug samples are shown in tracks 11 to 12 in Fig. 15. Measurements such as CRA, MICP, NMR, and 2D SEM analyses showed that Shilaif has low porosity of about 3% on average and very low permeability averaging 0.00057 mD. The porosity obtained from MICP and CRA analyses compared well with the core data derived from DE CT, and with the wireline logs (Track 11 in Fig. 15). The very low measured permeabilities from MICP and CRA experiments (Tracks 11 and 12 in Fig. 15) confirmed the tight nature of the rock along the core length.

The measured LECO TOC's are in-line with the TOC logs derived from DE CT and SGR data (Track 13 in Fig.15). Both data set showed that the Mid and Bottom of Shilaif have higher organic matter content than its top. The relatively high measured S_1 and S_2 in the middle and bottom of the formation is an indication of the prospectivity of these zones to produce hydrocarbons (Track 13 in Fig.15). The SARA analysis results plotted in Track 15 (Fig 15) indicated that the crude oil has low asphaltene components and abundant aromatics and resins along the core length. Also, the extractable organic matters (EOM) within the middle and bottom intervals (11619.12 ppm on average) are higher than those within the top of Shilaif (4638.01 ppm on average), proving the potentiality of both units, especially the Middle unit (Zone 2).

The 2D SEM-derived porosity and OM contents plotted in Fig.15 (Tracks 11 and 13, respectively) confirmed the petrophysical and geochemical findings and showed an average total porosity of (3.34 vol% volume) and OM content (5.77 wt % on average). Also, they demonstrated a good correspondence with the wireline data and confirmed the high prospectivity of Zone 2.

From the integration of core and plug data with the wireline logs, it can be concluded that Shilaif Formation in this well has a high prospective zone in the middle of the formation (Zone 2) and 2nd interval at the bottom of the core with less potentiality (Zone 3).

Further advance core analysis and well testing tests are recommended to enhance the source rock characterization of Shilaif Formation and define its economic potential appropriately.

Summary and Conclusions

The Cenomanian deposits of Shilaif Formation were studied using a comprehensive and integrative conventional and digital core analysis workflow to characterize its geological, geochemical, and petrophysical aspects and understand its hydrocarbon quality and production potentiality.
All the obtained conventional and digital core analysis results were integrated with the wireline logs to validate these logs, have a better understanding of the properties of Shilaif Formation and determine the best prospective units within Shilaif.
From the integration of core and plug data with the wireline logs, it can be concluded that Shilaif Formation in this well has a high prospective zone in the middle of the formation (Zone 2) and a second interval at the bottom of the core with less potentiality (Zone 3).
Zone 2 has the highest OM content in Shilaif (0.048 wt fraction, 0.096 v/v on average) and good porosity (0.09 v/v on average) and is made principally of carbonate minerals (calcite), followed by minor concentrations of clay minerals and silicates.
Zone 3 has OM content of 0.019 wt fraction (equivalent to ~0.038 v/v) on average and a porosity of 0.07 v/v on average, lower than the Zone 2. It is made mainly of carbonate followed by clay and silicates minerals.
Measurements such as CRA, MICP, NMR, and 2D SEM analyses showed that Shilaif has low porosity of about 3% on average and very low permeability averaging 0.00057 mD.
The LECO TOC measurements showed low OM content (poor potential) in the top of Shilaif (×034 ft- ×084 ft) and good OM content (excellent potential) towards the mid and bottom of Shilaif (×084 ft to ×129 ft) with an average of 4.78 wt% (equivalent to 9.56 vol%).
Pyrolysis analysis indicated a kerogen type I to II with an average Tmax equal to 431°C.
The relatively high measured S_1 and S_2 in the middle and bottom of the formation is an indication of their prospectivity to produce hydrocarbons.
The SARA analysis results indicated that the crude oil has low asphaltene components and abundant aromatics and resins along the core length.
The fluorescence of liptinite, and color of palynomorphs all suggest that the organic matter is early mature and within the early oil window.
Measured and calculated vitrinite reflectance (Ro) was, on average 0.59, confirming that the kerogen of Shilaif in the area of study falls within the immature to the early mature oil window.
Even though the 2D SEM images and NMR data confirmed the occurrence of the PAOM porosities in the mid and bottom of Shilaif, they are relatively less abundant compared to the total volume of the OM, especially towards its bottom, attributed to the low degree of transformation.
The full data integration was fundamental to evaluate the reservoir at different scales efficiently and rapidly, contributing to decision-making, data validation, and sweet spots identification.
Further advanced core analysis and well testing tests are recommended to enhance the source rock characterization of Shilaif Formation and define its economic potential.

Acknowledgments

The authors would like to thank the senior management of ADNOC and Halliburton for their kind support and the permission to publish this paper.

Abbreviation

BD	Bulk Density
CRA	Crushed Rock Analysis
CT	Computed Tomography

DE	Dual-energy
GR	Gamma Ray
HI	Hydrogen Index
MICP	Mercury Injection Capillary Pressure
NMR	Nuclear Magnetic Resonance
OM	Organic Matter
PE	Photoelectric Factor
PI	Production Index
Ro%	Vitrinite Reflectance
RTML	Rock Typing Machine Learning
SARA	Saturate, Aromatic, Resines, and Asphaltene Analysis
SGR	Spectral Gamma Ray
TOC	Total Organic Content
WL	Wireline
XRD	X-ray Diffraction
XRF	X-ray Fluorescence

Symbols

Ft	feet
g/cc	grams per cubic centimeter
mg HC/g	milligrams of hydrocarbon per gram
p.u.	porosity units
ppm	parts per million
vol%	percentage of volume
wt%	percentage of the total weight
%	percent
°C	degree Celsius

References

Almarzooq. A., AIGhamdi, T., Koronfol, S., Dernaika, M., Walls, J.;. Shale Gas Characterization and Property Determination by Digital Rock Physics, SPE-172840-MS, SPE Saudi Arabia Section Annual Technical Symposium and Exhibition, 21-24 April 2014.

Al-Zaabi, M., Taher, A., Azzam, I., Witte, J.; 2010. Geological Overview of the Middle Cretaceous Mishrif Formation in Abu Dhabi, SPE-137894, Abu Dhabi Petroleum Exhibition & Conference, 1-4 November 2010.

Bhatt, P., Zhunussova, G., Uluyuz, S., Baig, M., Makarychev, G., Mendez, A., Povstyanova, M.; 2018. Integrated Reservoir Characterization For Successful Hydraulic Fracturingin Organc Rich Unconventional Plays - A Case Study from UAE. SPE-192845-MS, Abu Dhabi Petroleum Exhibition & Conference, 12-15 November 2018.

Cantisano, M., Restrepo, D., Cespedes, S., Toelke, J., Grader, A., Suhrer, M., Walls, J.; 2013. Relative Permeability in a Shale Formation in Colombia Using Digital Rock Physics. SPE 168681/URTEC-1562626, Unconventional Resources Technology Conference, Denver, Colorado, 11-14 August 2013.

Dernaika, M., Al Jallad, O., Koronfol, S., Suhrer, M., Jing, W., Walls, J., Matar, S., Murthy, N., Zekraoui, M.; 2015. Petrophysical and Fluid Flow Properties of Tight Carbonate Source Rock Using Digital Rock Physics. SPE 178616-MS/URTeC:2154815. Unconventional Resources Technology Conference, San Antonio, Texas, 20-22 July 2015.

Dernaika, M., Walls, J., Koronfol, S., Al Jallad, O., & Sinclair, G. (2017, July 24). Petrophysical Properties of Shale From Different Source Rocks in the Middle East. Unconventional Resources Technology Conference. doi:10.15530/URTEC-2017-2667079

Fan, T., Wang, J., Buckley, J.; 2002. Evaluating Crude Oils by SARA Analysis. SPE-75228, SPE/DOE Improved Oil Recovery Symposium, 13-17 April 2002.

Grotsch, J., Suwaina, O., Ajlani, G., Taher, A., El-Khassawneh, R., Lokier, S., Coy, G., Van der Weerd, E., Masalmeh, S., Van Dorp, J.; 2003. The Arab Formation in central Abu Dhabi: 3D reservoir architecture and static and dynamic model. *GeoArabia*, Vol. **8**, No. 1, 2003.

Kausik, R., Fellah, K., Rylander, E., Singer, P. M., Lewis, R., and Sinclair, S.; 2015. NMR Relaxometry in Shale and Implications for Logging. SPWLA Annual Logging Symposium, 18-22 July, 2015.

Makarychev, G., Leyrer, K., Zeeshan, M., Van Laer, P.; 2018, Integration of Geochemical and Petrophysical Analysis for the Shilaif Formation Characterization. SPE-193331-MS, Abu Dhabi Petroleum Exhibition & Conference, 12-15 November 2018.

Morton-Thompson, Diana and Woods, Arnold M.; 1992. Development Geology Reference Manual. American Association of Petroleum Geologists, EBOOK: http://dx.doi.org/10.1306/Mthl0573

Peters, K. Cassa, M. R. 1994. Applied Source Rock Geochemistry. *AAPG Memoir* 60.

Stainer, S., Ahsan, S., Noufal, A., Franco, B., Koksalan, T., Ajmad, K., Helja, E., Alhosani, S., Adesanya, A.; 2015. Integrated Approach To Evaluate Unconventional and Tight Reservoirs in Abu Dhabi. SPE-177610-MS, Abu Dhabi Petroleum Exhibition & Conference, 9-12 November 2015.

Stainer, S, Raina, I, Dasgupta, S., Lewis, R., Monson, E. R., Abu-Snaineh, A., Alharti, A., Lis, G. P., Chertova, E.; 2015. Petrophysical Challenges in Unconventional and Tight Source Rocks, Onshore Abu Dhabi. SPE-17614-MS, Abu Dhabi Petroleum Exhibition & Conference, 9-12 November 2015.

Taher, A., 2010, Unconventional Oil Exploration Potential in Early Mature Source Rock Kitchens. SPE-137897, Abu Dhabi Petroleum Exhibition & Conference, 1-4 November 2010.

Tian, W., Jia, M., Xiao, D., Luo, B., Yang, J., Al Suwaidi, S., Ji, Y., LV, M., Shashanka, A., Mao, D., Hu, X.; 2019. Unconventional Oil Studies of Shilaif Source Rock in Western UAE. SPE-197729-MS, Abu Dhabi Petroleum Exhibition & Conference, 11-14 November 2019.

Tissot, B P., Durand, Welte, D. H.; 1984. Petroleum formation and occurance.

Van Laer, P., Leyrer, K., Povstyanova, M., Zeeshang, M., Makarychev, G., Al-Marzooqi, H.; 2019. Cenomanian Shilaif Unconventional Shale Oil Potential in onshore Abu Dhabi, UAE. URTeC 526, Unconventional Resources Technology Conference, 22-24 July 2019.

Walls, J. and Armbruster, M. 2012. Shale Reservoir Evaluation Improved by Dual-energy X-Ray CT Imaging: Technology Update. JPT, November.